Draft version December 8, 2023
Typeset using LaTeX **twocolumn** style in AASTeX631

PWN-powered Galactic Center X-ray filament G0.13-0.11: Proof of the synchrotron nature by IXPE

Eugene Churazov,[1,2] Ildar Khabibullin,[3,1,2] Thibault Barnouin,[4] Niccolò Bucciantini,[5,6,7] Enrico Costa,[8] Laura Di Gesu,[9] Alessandro Di Marco,[8] Riccardo Ferrazzoli,[8] William Forman,[10] Philip Kaaret,[11] Dawoon E. Kim,[8,12,13] Jeffery J. Kolodziejczak,[11] Ralph Kraft,[10] Frédéric Marin,[14] Giorgio Matt,[15] Michela Negro,[16] Roger W. Romani,[17] Stefano Silvestri,[18] Paolo Soffitta,[8] Rashid Sunyaev,[1,2] Jiri Svoboda,[19] Alexey Vikhlinin,[10] Martin C. Weisskopf,[11] Fei Xie,[20] Iván Agudo,[21] Lucio A. Antonelli,[22,23] Matteo Bachetti,[24] Luca Baldini,[25,26] Wayne H. Baumgartner,[11] Ronaldo Bellazzini,[25] Stefano Bianchi,[15] Stephen D. Bongiorno,[11] Raffaella Bonino,[27,28] Alessandro Brez,[25] Fiamma Capitanio,[8] Simone Castellano,[25] Elisabetta Cavazzuti,[9] Chien-Ting Chen,[29] Stefano Ciprini,[30,23] Alessandra De Rosa,[8] Ettore Del Monte,[8] Niccolò Di Lalla,[17] Immacolata Donnarumma,[9] Victor Doroshenko,[31] Michal Dovčiak,[32] Steven R. Ehlert,[11] Teruaki Enoto,[33] Yuri Evangelista,[8] Sergio Fabiani,[8] Javier A. García,[34] Shuichi Gunji,[35] Kiyoshi Hayashida,[36,*] Jeremy Heyl,[37] Wataru Iwakiri,[38] Svetlana G. Jorstad,[39,40] Vladimir Karas,[32] Fabian Kislat,[41] Takao Kitaguchi,[33] Henric Krawczynski,[42] Fabio La Monaca,[8,43,12] Luca Latronico,[27] Ioannis Liodakis,[11] Simone Maldera,[27] Alberto Manfreda,[44] Andrea Marinucci,[9] Alan P. Marscher,[39] Herman L. Marshall,[45] Francesco Massaro,[27,28] Ikuyuki Mitsuishi,[46] Tsunefumi Mizuno,[47] Fabio Muleri,[8] Chi-Yung Ng,[48] Stephen L. O'Dell,[11] Nicola Omodei,[17] Chiara Oppedisano,[27] Alessandro Papitto,[22] George G. Pavlov,[49] Abel L. Peirson,[17] Matteo Perri,[23,22] Melissa Pesce-Rollins,[25] Pierre-Olivier Petrucci,[50] Maura Pilia,[24] Andrea Possenti,[24] Juri Poutanen,[51] Simonetta Puccetti,[23] Brian D. Ramsey,[11] John Rankin,[8] Ajay Ratheesh,[8] Oliver J. Roberts,[29] Carmelo Sgrò,[25] Patrick Slane,[10] Gloria Spandre,[25] Douglas A. Swartz,[29] Toru Tamagawa,[33] Fabrizio Tavecchio,[52] Roberto Taverna,[53] Yuzuru Tawara,[46] Allyn F. Tennant,[11] Nicholas E. Thomas,[11] Francesco Tombesi,[43,30,54] Alessio Trois,[24] Sergey S. Tsygankov,[51] Roberto Turolla,[53,55] Jacco Vink,[56] Kinwah Wu,[55,8] and Silvia Zane[55]

[1] *Max Planck Institute for Astrophysics, Karl-Schwarzschild-Str. 1, D-85741 Garching, Germany*
[2] *Space Research Institute (IKI), Profsoyuznaya 84/32, Moscow 117997, Russia*
[3] *Universitäts-Sternwarte, Fakultät für Physik, Ludwig-Maximilians-Universität München, Scheinerstr.1, 81679 München, Germany*
[4] *Observatoire Astronomique de Strasbourg, UMR 7550, 67000 Strasbourg, France*
[5] *INAF Osservatorio Astrofisico di Arcetri, Largo Enrico Fermi 5, 50125 Firenze, Italy*
[6] *Dipartimento di Fisica e Astronomia, Università degli Studi di Firenze, Via Sansone 1, 50019 Sesto Fiorentino (FI), Italy*
[7] *Istituto Nazionale di Fisica Nucleare, Sezione di Firenze, Via Sansone 1, 50019 Sesto Fiorentino (FI), Italy*
[8] *INAF Istituto di Astrofisica e Planetologia Spaziali, Via del Fosso del Cavaliere 100, 00133 Roma, Italy*
[9] *Agenzia Spaziale Italiana, Via del Politecnico snc, 00133 Roma, Italy*
[10] *Center for Astrophysics, Harvard & Smithsonian, 60 Garden St, Cambridge, MA 02138, USA*
[11] *NASA Marshall Space Flight Center, Huntsville, AL 35812, USA*
[12] *Dipartimento di Fisica, Università degli Studi di Roma "La Sapienza", Piazzale Aldo Moro 5, 00185 Roma, Italy*
[13] *Dipartimento di Fisica, Università degli Studi di Roma "Tor Vergata", Via della Ricerca Scientifica 1, 00133 Roma, Italy*
[14] *Université de Strasbourg, CNRS, Observatoire Astronomique de Strasbourg, UMR 7550, 67000 Strasbourg, France*
[15] *Dipartimento di Matematica e Fisica, Università degli Studi Roma Tre, Via della Vasca Navale 84, 00146 Roma, Italy*
[16] *Department of Physics and Astronomy, Louisiana State University, Baton Rouge, LA 70803, USA*
[17] *Department of Physics and Kavli Institute for Particle Astrophysics and Cosmology, Stanford University, Stanford, California 94305, USA*
[18] *Istituto Nazionale di Fisica Nucleare, Sezione di Pisa, Largo B. Pontecorvo 3, I-56127 Pisa, Italy*
[19] *Astronomical Institute of the Czech Academy of Sciences, Boční II 1401/1, 14100 Praha 4, Czech Republic*
[20] *Guangxi Key Laboratory for Relativistic Astrophysics, School of Physical Science and Technology, Guangxi University, Nanning 530004, China*
[21] *Instituto de Astrofísica de Andalucía – CSIC, Glorieta de la Astronomía s/n, 18008 Granada, Spain*
[22] *INAF Osservatorio Astronomico di Roma, Via Frascati 33, 00040 Monte Porzio Catone (RM), Italy*
[23] *Space Science Data Center, Agenzia Spaziale Italiana, Via del Politecnico snc, 00133 Roma, Italy*
[24] *INAF Osservatorio Astronomico di Cagliari, Via della Scienza 5, 09047 Selargius (CA), Italy*
[25] *Istituto Nazionale di Fisica Nucleare, Sezione di Pisa, Largo B. Pontecorvo 3, 56127 Pisa, Italy*
[26] *Dipartimento di Fisica, Università di Pisa, Largo B. Pontecorvo 3, 56127 Pisa, Italy*
[27] *Istituto Nazionale di Fisica Nucleare, Sezione di Torino, Via Pietro Giuria 1, 10125 Torino, Italy*
[28] *Dipartimento di Fisica, Università degli Studi di Torino, Via Pietro Giuria 1, 10125 Torino, Italy*
[29] *Science and Technology Institute, Universities Space Research Association, Huntsville, AL 35805, USA*
[30] *Istituto Nazionale di Fisica Nucleare, Sezione di Roma "Tor Vergata", Via della Ricerca Scientifica 1, 00133 Roma, Italy*
[31] *Institut für Astronomie und Astrophysik, Universität Tübingen, Sand 1, 72076 Tübingen, Germany*
[32] *Astronomical Institute of the Czech Academy of Sciences, Boční II 1401/1, 14100 Praha 4, Czech Republic*
[33] *RIKEN Cluster for Pioneering Research, 2-1 Hirosawa, Wako, Saitama 351-0198, Japan*
[34] *X-ray Astrophysics Laboratory, NASA Goddard Space Flight Center, Greenbelt, MD 20771, USA*

[35] Yamagata University,1-4-12 Kojirakawa-machi, Yamagata-shi 990-8560, Japan
[36] Osaka University, 1-1 Yamadaoka, Suita, Osaka 565-0871, Japan
[37] University of British Columbia, Vancouver, BC V6T 1Z4, Canada
[38] International Center for Hadron Astrophysics, Chiba University, Chiba 263-8522, Japan
[39] Institute for Astrophysical Research, Boston University, 725 Commonwealth Avenue, Boston, MA 02215, USA
[40] Department of Astrophysics, St. Petersburg State University, Universitetsky pr. 28, Petrodvoretz, 198504 St. Petersburg, Russia
[41] Department of Physics and Astronomy and Space Science Center, University of New Hampshire, Durham, NH 03824, USA
[42] Physics Department and McDonnell Center for the Space Sciences, Washington University in St. Louis, St. Louis, MO 63130, USA
[43] Dipartimento di Fisica, Università degli Studi di Roma "Tor Vergata", Via della Ricerca Scientifica 1, 00133 Roma, Italy
[44] Istituto Nazionale di Fisica Nucleare, Sezione di Napoli, Strada Comunale Cinthia, 80126 Napoli, Italy
[45] MIT Kavli Institute for Astrophysics and Space Research, Massachusetts Institute of Technology, 77 Massachusetts Avenue, Cambridge, MA 02139, USA
[46] Graduate School of Science, Division of Particle and Astrophysical Science, Nagoya University, Furo-cho, Chikusa-ku, Nagoya, Aichi 464-8602, Japan
[47] Hiroshima Astrophysical Science Center, Hiroshima University, 1-3-1 Kagamiyama, Higashi-Hiroshima, Hiroshima 739-8526, Japan
[48] Department of Physics, The University of Hong Kong, Pokfulam, Hong Kong
[49] Department of Astronomy and Astrophysics, Pennsylvania State University, University Park, PA 16801, USA
[50] Université Grenoble Alpes, CNRS, IPAG, 38000 Grenoble, France
[51] Department of Physics and Astronomy, 20014 University of Turku, Finland
[52] INAF Osservatorio Astronomico di Brera, via E. Bianchi 46, 23807 Merate (LC), Italy
[53] Dipartimento di Fisica e Astronomia, Università degli Studi di Padova, Via Marzolo 8, 35131 Padova, Italy
[54] Department of Astronomy, University of Maryland, College Park, Maryland 20742, USA
[55] Mullard Space Science Laboratory, University College London, Holmbury St Mary, Dorking, Surrey RH5 6NT, UK
[56] Anton Pannekoek Institute for Astronomy & GRAPPA, University of Amsterdam, Science Park 904, 1098 XH Amsterdam, The Netherlands

ABSTRACT

We report the discovery of X-ray polarization from the X-ray-bright thread/filament G0.13-0.11 in the Galactic Center region. This filament features a bright hard X-ray source, most plausibly a Pulsar Wind Nebula (PWN), and an extended and structured diffuse component. Combining the polarization signal from IXPE with the imaging/spectroscopic data from Chandra, we find that X-ray emission of G0.13-0.11 is highly polarized PD=57(±18)% in the 3-6 keV band, while the polarization angle is PA=21°(±9°). This high degree of polarization proves the synchrotron origin of the X-ray emission from G0.13-0.11. In turn, the measured polarization angle implies that the X-ray emission is polarized approximately perpendicular to a sequence of non-thermal radio filaments that may be part of the Galactic Center Radio Arc. The magnetic field of the order of 100 μG appears to be preferentially ordered along the filaments. The above field strength is the fiducial value that makes our model self-consistent, while the other conclusions are largely model-independent.

1. INTRODUCTION

The origin of spectacular radio filaments/threads (including the most prominent Radio Arc) in the Galactic Center region and the role of pulsar wind nebulae (PWNe) in their appearance is an actively debated topic (e.g. Yusef-Zadeh et al. 2004). Many of the observed radio filaments have spectral and polarization properties suggesting that they are dominated by non-thermal emission (e.g Yusef-Zadeh et al. 1984; Tsuboi et al. 1986; Lang et al. 1999; LaRosa et al. 2004; Heywood et al. 2019). Hereafter, we refer to them as nonthermal filaments (NTFs).

Some of the NTFs have known X-ray counterparts. Here, we focus on one of them – an X-ray/radio thread G0.13-0.11. In the X-ray band, G0.13-0.11 was studied by Yusef-Zadeh et al. 2002; Wang et al. 2002, and Zhang et al. 2020 using Chandra and NuSTAR data. The case of G0.13-0.11 is especially interesting due to the close correspondence of X-ray structures and a subsystem of the Radio Arc filaments noted by Yusef-Zadeh et al. (2002). Based on a filamentary X-ray appearance, the presence of a compact source, and a non-thermal spectrum, the latter two studies focused on the interpretation of G0.13-0.11 as a PWN with a filament formed by leptons escaping from the supersonically moving PWN into the ambient magnetic field (see, e.g., Gaensler & Slane 2006; Kargaltsev et al. 2017; Bykov et al. 2017; Olmi & Bucciantini 2023, for reviews).

In this class of models, known as Bow Shock PWN (BSPWN), the leptons with sufficiently large Lorentz factor (hence large gyroradius) can cross the bow shock region and escape the source (Bandiera 2008). Bykov et al. 2017 (see their Section 6) discussed conditions needed to produce very hard spectra (dominated by the highest energies) and a reconnection scenario that can lead to asymmetric or one-

* Deceased

sided X-ray structures observed in several BSPWNs, such as Lighthouse (Pavan et al. 2011) or Guitar (de Vries et al. 2022) nebulae. In this scenario, the mutual orientation of the PWN and the ambient magnetic fields set the topology of the field lines in a way reminiscent of Earth's magnetosphere embedded in the Solar wind. Numerical magneto-hydrodynamical (MHD) models of these objects appear to be in reasonable agreement with observations (e.g. Barkov et al. 2019; Olmi & Bucciantini 2019). In these models, the radio and X-ray fluxes from threads are produced by synchrotron emission of relativistic leptons and hence should be polarized, if the magnetic field is at least partly ordered. Now IXPE (Weisskopf et al. 2022) can test this prediction in the X-ray regime. In the X-ray regime, the Polarization Angle (PA) is expected to be perpendicular to the orientation of the magnetic field and, unlike the radio data (e.g. Paré et al. 2019, 2021), it is not affected by the Faraday rotation and depolarization due to foreground magnetized plasma.

2. DATA

In this paper, we used the data of two IXPE observations of the Galactic Center region, more specifically, a complex of molecular clouds ~ 0.1 degrees to the East of Sgr A* (Marin et al. 2023). These observations with a total clean exposure time of 1.8 Msec, were performed in two parts - in February 2022 and September 2023. These two observations were centered on (RA,Dec) (266.51,-28.89) and (266.57,-28.89), respectively, with an offset between them of ~ 3′. The data were processed with the standard IXPE pipeline. The output FITS files of this pipeline contain the event-by-event Stokes parameters (see Kislat et al. 2015) from which the polarization observables of the X-ray radiation can be derived. The data products are publicly available for use by the international astrophysics community at the High-Energy Astrophysics Science Archive Research Center (HEASARC, at the NASA Goddard Space Flight Center). To these level-2 event files, an energy-dependent particle background rejection algorithm based on photoelectron-track ellipticity was applied that allows removal of up to ~ 40% of the instrumental background (Di Marco et al. 2023). In addition, observation times affected by increased background due to Solar activity were removed (see Marin et al. 2023, for additional details on the procedure).

High spatial resolution X-ray images were obtained with Chandra over multiple observing campaigns in 2000-2022. The total exposure of the Chandra pointings with G0.13–0.11 located in the central region of the Field of View (FOV) with high spatial resolution is 1.4 Msec. The Chandra data reduction follows a standard procedure based on the latest versions of the data reduction software (CIAO v. 4.14) and calibration (CALDB v. 4.9.8). Our particular approach and analysis steps are described in detail in Vikhlinin et al. (2009). Briefly, they include identification and removal of high background periods, correction of photon energies for the time and detector temperature dependence of the charge transfer inefficiency and gain, and creation of matching background datasets using blank sky observations with exposure times similar to the Galactic Center pointings. For the analysis presented here, we use the combined flat-fielded and background-subtracted Chandra image in the 2–8 keV band, and spectra extracted in several elliptical regions, as described below. Following the standard approach for analysing Chandra spectra of extended sources, we have generated the spectral response files that combine the position-dependent ACIS calibration with the weights proportional to the observed brightness.

In the radio band, we used publicly available MeerKAT images[1] at the central frequency of 1.3 GHz and ~ 6″ angular resolution (see Heywood et al. 2022, for a detailed description).

Fig. 1 shows a combination of the Chandra X-ray image in the 2.3-8 keV band (in green) and the MeerKAT radio image (in red). G0.13-0.11 is a green feature to the right of a triangular-shaped sequence of NTFs near the center of the image. The cyan lines show the Polarization Angle of the G0.13-0.11 X-ray emission (best-fitting value $\pm 1\sigma$ error) measured by IXPE.

3. X-RAY IMAGES AND SPECTRA

The X-ray images of the G0.13-0.11 region in the 2-8 keV band obtained by IXPE and Chandra are shown in Fig. 2. The images were smoothed with a Gaussian filter with $\sigma = 5''$ and $0.5''$ for IXPE and Chandra, respectively. G0.13-0.11 is located in the bottom-left corner of the image and is clearly visible as a pair of bright wings in the Chandra image. Sgr A* is outside of the region shown, ~ 0.06 degrees from the right boundary.

With the approach outlined above, IXPE will provide the polarized emission (Q and U spectra) of the entire region, while Chandra data resolve the spectrum into spatially distinct components, in particular, the non-thermal component. The Chandra image with the additional regions used for spectra extraction is shown in Fig. 3, including a point source CXOGCS J174621.5-285256 marked with the blue circle ("SRC"), two narrow green boxes covering the brightest part of the box-shaped structure ("Wings-n"), a larger red ellipse that covers the "wings" and a more extended structure to the left from the wings ("Wings-e"), and the entire "IXPE" region (black). The latter region ($\approx 43 \times 60''$) is the same as shown in Fig. 2. In the 2022 and 2023 IXPE observations, the "IXPE" region was ~ 4 and ~ 1.8 arcminutes from the center of the instrument FoV, respectively. Note that while the IXPE instrumental half-power diameter (HPD) is 25", flex-

[1] https://doi.org/10.48479/fyst-hj47

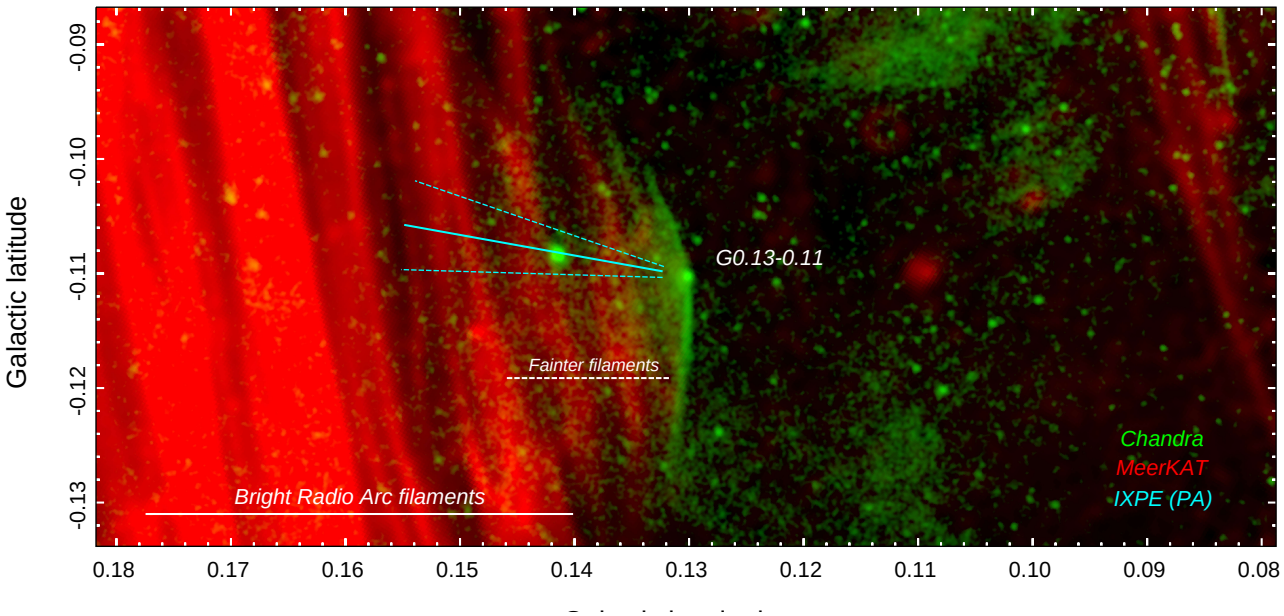

Figure 1. A combination of radio (MeerKAT; 1.3 GHz, red) and X-ray (Chandra; 2.3-8 keV, Log scale, smoothed with $\sigma = 0.5''$ Gaussian, green) images of the G0.13-0.11 region in Galactic coordinates. The prominent red vertical threads on the left side of the image belong to the NTFs of the Radio Arc. G0.13-0.11 is the green feature to the east of a sequence of fainter NTFs near the center of the image. G0.13-0.11 consists of (i) a compact core (the bright green dot at the center of the figure), presumably the pulsar itself and its PWN, (ii) a pair of bright "wings", and (iii) a more diffuse (possibly structured) X-ray glow to the left of the "wings" (at higher Galactic longitude). The cyan lines show the Polarization Angle (PA) of the G0.13-0.11 emission (best-fitting value $\pm 1\sigma$ error, i.e. 21 ± 9 degrees) measured by IXPE. The polarization direction is approximately perpendicular to the X-ray "wings" and the nearest NTFs. Coupled with the large polarization degree, this proves that X-rays are produced by synchrotron emission of $\sim$ TeV electrons.

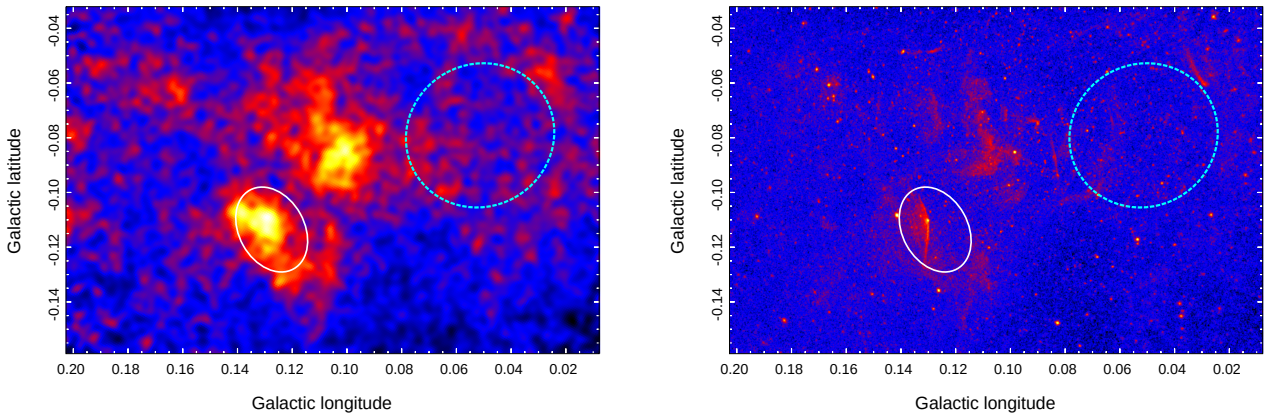

Figure 2. 3-6 keV IXPE (left panel) and Chandra (right panel) X-ray images. Two elliptical regions were used for spectra extraction. The white ellipse covers the G0.13-0.11 area. Given the uncertainties with the IXPE astrometry, a relatively large region was selected guided by the IXPE image. The bigger cyan region was used as a background region for spectral analysis. The Chandra image is in logarithmic scale to show more clearly bright point sources and faint diffuse emission. For the IXPE image, a linear scale is used.

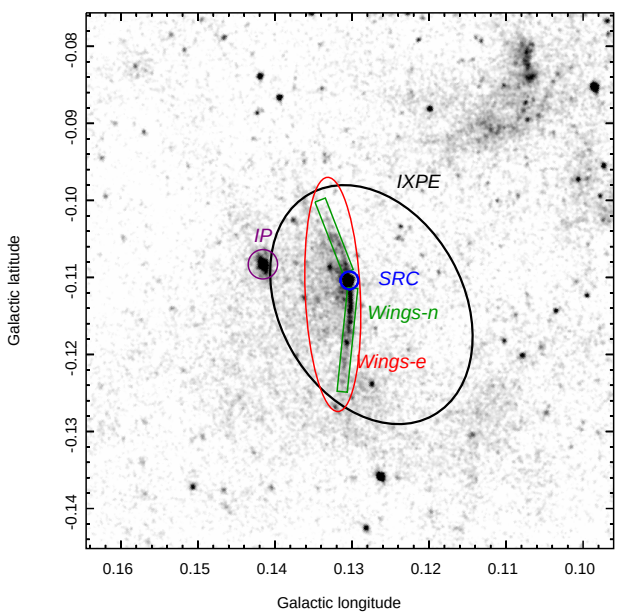

Figure 3. Regions used for spectral extraction from the Chandra data. The black ellipse called "IXPE" is the same as the source region in Fig. 2. The other three regions ("SRC", "Wings-n" and "Wings-e") cover the compact source and the brighter parts of the X-ray bow. The "SRC" and "Wings-n" regions do not overlap. Larger regions ("Wings-e" and "IXPE") include all the Chandra counts inside them, i.e., the "IXPE" region includes the counts from "SRC", "Wings-n", and almost the entire "Wings-e" counts. The purple circle labelled as "IP" shows the extraction region for the Intermediate Polar CXOUGC J174622.7–285218.

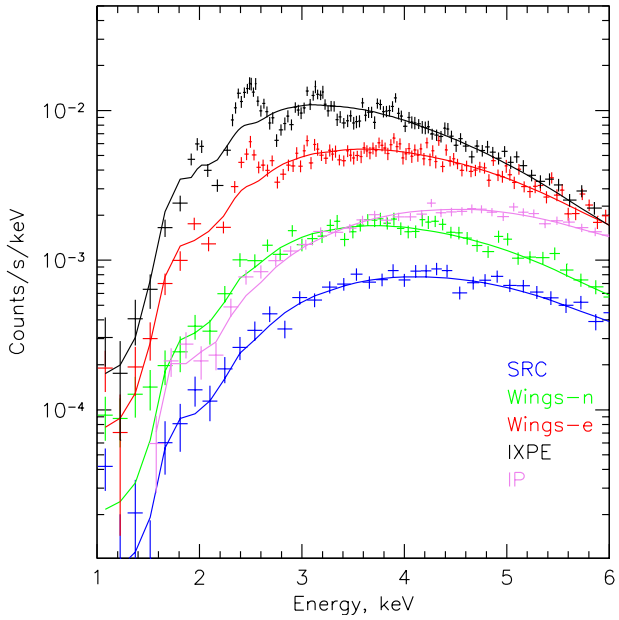

Figure 4. Background subtracted Chandra spectra in the vicinity of G0.13-0.11. The colors correspond to the regions shown in Fig. 3 and are identified in this figure. The solid lines show the best-fitting absorbed power-law model fits to these spectra. While a pure power law can reasonably well describe the compact source spectrum (blue), other regions clearly contain a non-negligible contribution of thermal emission that gives rise to emission lines at low energies. The spectrum of the intermediate polar CXOUGC J174622.7–285218 is shown in purple.

ure and aspect jitter always somewhat blur the images. While this can be largely removed during typical IXPE observations of bright point sources, in fields with faint extended emission aspect correction is more difficult. Despite extra care in aligning the images, such blur doubtless remains and so we adopt generous extraction apertures. This should help to collect most of the photons from the polarized source and make the resulting spectrum less sensitive to the exact positioning of the extraction region. The spectra extracted from the Chandra data (corrected for the background extracted from the almost circular region ($\approx 100 \times 94''$) shown with the dashed line in Fig. 2) are shown in Fig. 4. The diffuse X-ray emission of the Galactic Center region consists of several spectral components, some of which are highly variable in space and time and contain bright emission lines, e.g. the lines at 6.4 and 6.7 keV of neutral and He-like iron. The former line is due to the reflection of X-rays by the neutral/molecular medium (e.g. Vainshtein & Sunyaev 1980; Koyama et al. 1996), while the latter is a combination of numerous accreting stellar mass objects that produce "thermal" spectra (e.g. Revnivtsev et al. 2009). This means that there is no well-defined and "optimal" choice of the background region. Since in this study, we are interested in the non-thermal component, the background region was selected to have a comparable mix of the reflection and thermal spectra. No fine-tuning was done when selecting the background region although we have verified that other reasonable choices do not significantly affect our final results. To mitigate the uncertainties associated with the contributions of the reflection component above 6 keV and strong lines below 3 keV coupled with strong low-energy photoelectric absorption, we restrict the analysis of IXPE data to the 3-6 keV band. The higher energy resolution of Chandra permits the spectral analysis in a broader band, illustrating strong suppression of X-ray flux below 2-3 keV due to photo-electric absorption with a typical column density $N_{\rm H} \sim 8\,10^{22}\,{\rm cm}^{-2}$ (see Table 1).

Simple absorbed power-law model fits to the spectra are shown with solid lines. Clearly, strong emission lines (e.g., of strongly ionized Si or S) are present in the Chandra spectrum of the "IXPE" region even after subtracting the spectrum extracted from the background region. Somewhat weaker lines are still seen in the "Wings-e" spectrum, while the "Wings-n" and "SRC" spectra seem to be reasonably well described by the power law model.

The parameters of the model are given in Table 1. The central bright source, presumably the pulsar itself and possibly a compact part of its PWN, has the hardest spectrum $\Gamma \sim 1.35$,

Table 1. Absorbed power-law model fits to the spectrum of the Chandra spectra for three regions of G0.11-0.13 (see Fig. 3 for regions definition). The observed 2-10 keV fluxes (i.e. including the effects of the low-energy photoelectric absorption) are quoted.

Region	N_H 10^{22} cm^{-2}	Γ	$F_{2-10\,keV}$ erg s^{-1} cm^{-2}	Area arcsec^2	χ^2 (d.o.f.)
"SRC"	7.7 ± 0.6	1.35 ± 0.14	$1.1\,10^{-13}$	54	465 (478)
"Wings-n"	7.6 ± 0.4	2.27 ± 0.12	$1.6\,10^{-13}$	420	506 (478)
"Wings-e"	7.1 ± 0.2	2.40 ± 0.07	$5.0\,10^{-13}$	2213	645 (478)
Entire "IXPE" region	8.1 ± 0.2	3.75 ± 0.07	$6.4\,10^{-13}$	8000	1010 (478)

while the Wings-n and Wings-e regions have significantly softer spectra $\Gamma \sim 2.2 - 2.4$. Broadly, these spectral parameters are consistent with those obtained by Yusef-Zadeh et al. (2002) and Wang et al. (2002), given the difference in the choice of extraction regions and possible variability of the diffuse (reflected) emission. The "IXPE" region is clearly contaminated by thermal emission below 3-4 keV. However, already at ~ 5 keV, the fluxes from the "Wings-e" and "IXPE" regions are comparable. The "Wings-e" spectrum itself contains a non-negligible fraction of thermal emission. To set a lower limit on the degree of polarization, we conservatively assume that the total intensity (i.e. Stokes $I(E)$) of the non-thermal component is described by the "Wings-e" spectrum (the red lines in Fig. 4). We, therefore, model the IXPE's $Q(E)$ and $U(E)$ spectra, assuming that $I(E)$ is known. With this approach, there are only two free parameters: the degree of polarization P and the polarization direction ϕ. When fitting $Q(E)$ and $U(E)$ spectra, these parameters enter as prefactors $P\cos 2\phi$ and $P\sin 2\phi$ in front of the Chandra $I(E)$ model convolved with the IXPE response to polarized emission. Fig. 5 shows the I,Q, and U spectra obtained by IXPE, along with Chandra's "Wings-e" model convolved with the IXPE response. The IXPE response was averaged over three IXPE modules.

The above assumptions yield the following best-fitting values: PD =57 ± 18% and angle PA =21 ± 9 degrees. Setting PD = 0 increases the value of χ^2 by 10.37, which for 2 degrees of freedom implies a probability $\sim 5.3 \times 10^{-3}$ of a random fluctuation. The corresponding confidence contours are shown in Fig. 6. The high value of the PD is a strong argument in favor of the synchrotron origin of the X-ray emission. The constraints on the polarization angle are shown in Fig.1. Within uncertainties, the polarization plane is perpendicular to the bright X-ray structure and, also, to the direction of radio filaments co-spatial with the extended X-ray source. This suggests that both the radio and X-ray emissions are due to the synchrotron radiation of relativistic electrons in the same magnetic structures.

We note here, that when calculating the degree of polarization, we conservatively assumed that essentially all non-thermal flux coming from the "IXPE" region is polarized

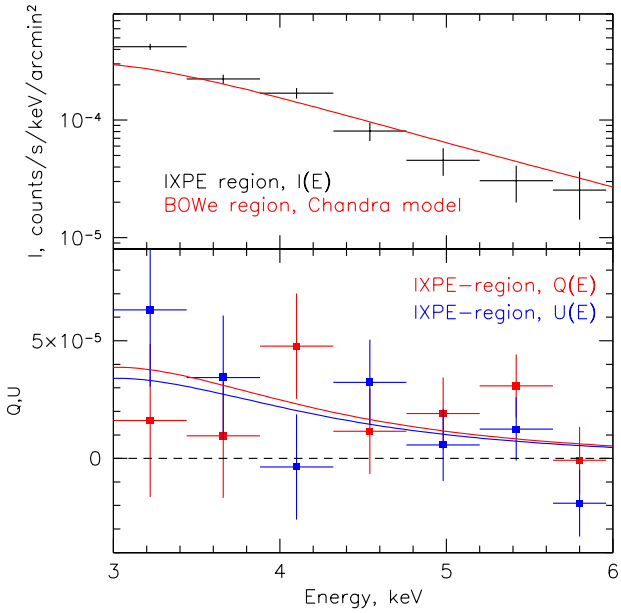

Figure 5. IXPE spectra. **Top panel:** IXPE total background-subtracted Stokes $I(E)$ spectrum in the 3-6 keV band from the "IXPE" region (see Fig. 2 and 3) is shown with the black points. The red line in the top panel shows Chandra's "Wings-e" region model (see Fig.4) convolved with the IXPE response. **Bottom panel:** Stokes $Q(E)$ and $U(E)$ spectra of the "IXPE" region - red and blue points, respectively. The solid lines show the expected spectra for Chandra's "Wings-e" model and the best-fitting polarization degree PD =57 ± 18% and angle PA =21 ± 9 degrees.

(i.e. model "Wings-e"). If instead, only the emission coming from the "Wings-n" region or from the PWN itself is polarized, then the degree of polarization will only be higher. For instance, substituting the Chandra-based "Wings-e" model with the "Wings-n" model for $I(E)$, yields PD=160 ± 60%. A high degree of polarization (> 100%) is a plausible outcome of using the incorrect assumption of what fraction of the total signal comes from the polarized source. Apart from the statistical errors already included in the uncertainties of PD estimates, there might be additional uncertainties associated with the limited astrometric quality of IXPE data, although our choice of a large region for spectral extraction will have minimized these uncertainties. To this end, we note that

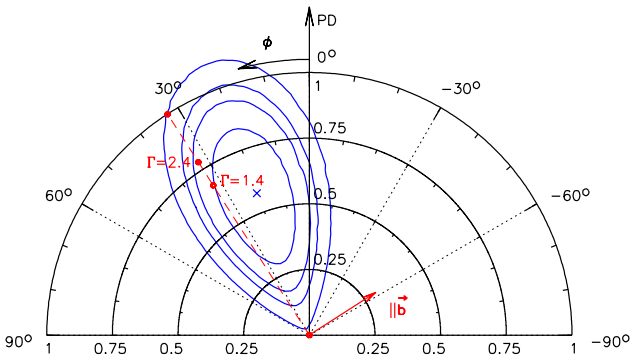

Figure 6. Confidence regions for the polarization degree (PD) and polarization angle (PA, equatorial coordinate system) derived from the IXPE data, assuming that the polarized emission corresponds to the "Wings-e" spectral model. The blue line shows the contours of the χ^2 statistic after subtraction of the minimum value $\chi^2_{\rm min}$ reached at PD≈0.57 and PA≈ 21° (marked with a blue cross). The contours show $\Delta\chi^2$ =2.3, 4.61, 6.17, and 9.21 levels, corresponding to 68.3%(1σ), 90%, 95.4% (2σ), and 99% confidence levels, respectively. The red dashed line illustrates the expected PA in the case, when the electric field vector is parallel to the Galactic plane, and two circles mark the maximum polarization for synchrotron emission for Γ = 1.4 and 2.4 (as labelled next to them). The outmost contour extends to PD values larger than 1. This is a plausible outcome of our procedure when the $Q(E)$ and $U(E)$ data are taken from IXPE, while $I(E)$ is based on the Chandra data extracted from a smaller region which is supposed to be polarised and might not coincide with true polarized $I(E)$ seen by IXPE.

the presence of the bright and time-variable Intermediate Polar CXOUGC J174622.7–285218 (Muno et al. 2009) in close vicinity of G0.13-0.11 (see Fig. 3) can be considered as a possible source of the polarized signal contamination for IXPE. However, as evident from Fig. 4, its flux at ∼ 4 keV is similar to that of the "Wings-n" region. This means that if this IP is the dominant source of polarization, its emission should be almost 100% polarized, which is unlikely. For example, Matt (2004) estimated the maximum degree of polarization in magnetic Cataclysmic Variables of about 4% produced by scattering of the thermal radiation.

4. DISCUSSION & CONCLUSIONS

IXPE data provide two main observational results: (i) strong polarization of G0.13-11 X-ray emission, PD =57 ± 18%, and (ii) polarization direction almost along the Galactic Plane. This directly proves that X-ray emission is of synchrotron origin and that the orientation of the magnetic field follows a subsystem of the Radio Arc NTFs[2], which are elongated perpendicular to the Galactic Plane. These statements are essentially model-independent.

These data also prove that the field is well-ordered. Indeed, for a perfectly aligned magnetic field and a power law distribution of relativistic leptons over energy $\propto \gamma^{-p}$ with index p, the degree of the synchrotron emission polarisation is (e.g. Longair 2011)

$$\mathrm{PD}_{\rm max} = \frac{3p+3}{3p+7} = \frac{3\Gamma}{3\Gamma+2}, \qquad (1)$$

where $\Gamma = (p+1)/2$ is the photon index of the observed spectrum (for Γ between 1.4 and 2.2, the maximum degree of polarization is between 68 and 78%). By using the formulation for depolarization of synchrotron emission in a turbulent magnetic field by Bandiera & Petruk (2016) we estimated a ratio of turbulent versus ordered magnetic field energy to be likely smaller than ∼ 1.5. However, the observed PD= 57 ± 18% is consistent (within uncertainties) even with a perfectly ordered field (see Fig. 6). Notice that a high level of polarization can be achieved even in a fully turbulent regime if the turbulence is anisotropic (typically at a level 2-to-4), given that polarization is sensitive to the alignment of the magnetic field with a certain direction and is insensitive to field reversals (Bandiera & Petruk 2016). This preferred direction should be maintained across the IXPE spectral extraction region. Indeed current models of X-ray emission in bright jet-like features associated with PSRs advocate amplification of the magnetic field via some form of streaming instability, to justify magnetic field values that are typically inferred to be an order of magnitude higher than the surrounding ISM (Bandiera 2008). This might not be needed in the GC environment, where the ambient magnetic field can be high.

The X-ray emission of G0.13-0.11 is co-spatial with a Fermi source 4FGL J1746.4-2852 (Abdollahi et al. 2020) at GeV energies and a TeV-source HESS J1746–285 (H. E. S. S. Collaboration et al. 2018). The standard leptonic model for broadband radio-TeV objects usually relies on two processes: the synchrotron and Inverse Compton (IC) emissions. We defer an in-depth discussion for a forthcoming publication but note that the following set of fiducial parameters might explain some of the main characteristics of the G0.13-0.11 broadband spectrum: $B \sim 100\,\mu$G relevant for the radio–X-ray regime (synchrotron emission) and a combination of the CMB plus local ∼eV radiation field with the energy density of the order of 100 eV cm^{-3} (e.g. Popescu et al. 2017; Niederwanger et al. 2019) for the photons in the GeV-TeV range produced via

[2] The large Faraday rotation measure RM ∼ a few 10^3 rad m^{-2} (e.g. Paré et al. 2019, 2021) severely affects the PA determination at radio frequencies and limits reliable polarization measurements to patches of the brightest radio filaments. In contrast, polarization in the X-ray regime does not suffer from Faraday rotation.

Inverse Compton scatterings. Such a value of the magnetic field strength agrees with the equipartition arguments (e.g. Beck & Krause 2005) based on the measured X-ray flux and the broad-band photon index $\Gamma = 2$, although allowing the index to vary between 1.6 and 2.4 changes B between ~ 20 and $\sim 800\,\mu$G, respectively (see, e.g. Morris 2006, for discussion of various arguments in favor of weaker and stronger fields). The adopted value of $B \sim 100\,\mu$G implies that the field energy density is of the same order as the energy density of the radiation and, therefore, the lifetime of leptons emitting at a given frequency is close to the maximum. In this case, X-rays are produced by the leptons with $\gamma \sim 3 \times 10^7$ which have a lifetime consistent with the size of G0.13-0.11, provided that they can propagate with a sizable fraction (~ 0.2) of the speed of light. For photons with TeV energies, produced by IC scattering of ~eV photons, the cross-section is already subject to the Klein-Nishina suppression, while for the CMB photons, the scattering is still in the Thomson regime where the cross-section is maximal.

In connection with the fast propagation of relativistic electrons along a filament with a rather strong magnetic field, we note an interesting possible similarity with galaxy clusters, where extended structures in the radio bands are observed both in the cores and outskirts (e.g. Brienza et al. 2021; Rudnick et al. 2022). These structures often have very similar spectral properties (e.g. Rajpurohit et al. 2020). This suggests that relativistic electrons are able to propagate along the filament with velocities significantly larger than the sound or Alfven speeds in the bulk of the thermal intracluster medium (Churazov et al. 2023). The filaments in both classes of objects might be threads of a strong magnetic field embedded in the medium with a weaker magnetic field. This does not exclude possible amplification of the magnetic field by streaming particles from the PSR.

Apart from the polarized synchrotron X-ray emission of G0.13-0.11, there are many more radio and (fainter) X-ray threads in the same region that are visible in Chandra data. Presumably, they are polarized too and, therefore, can contribute to the overall polarization signal from the Galactic Center region. It is also possible that even fainter threads are present that are too weak to be detected individually. Since the direction of polarization might be set by the ambient magnetic field, this background polarization signal will also be polarized along the Galactic Plane (at least in the areas where "vertical" NTFs are present).

Yet another source of polarized emission is the Compton-scattered emission of the Sgr A* flare(s) that happened some hundreds of years ago. This scenario, motivated by the observed hard X-ray continuum and fluorescent lines of neutral iron from dense molecular clouds, was put forward in the 90s (Sunyaev et al. 1993; Markevitch et al. 1993; Koyama et al. 1996). If the continuum emission is scattered light from Sgr A*, it has to be polarized (Churazov et al. 2002) perpendicular to the direction towards Sgr A*. A weak polarized emission from the area within a few arcminutes from G0.13-0.11 was indeed detected in the first IXPE observations of the GC region (Marin et al. 2023). The emission from G0.13-0.11 itself was excluded in that analysis to avoid potential contamination. Now we see that there was a good reason to do so. Somewhat ironically, the polarization angles from X-ray threads and reflection are approximately orthogonal to each other and, therefore, can attenuate the net polarization signal if combined. The presence of many faint polarized threads is, therefore, a complication (an interesting one!) for the analysis of IXPE data from the GC. The limited astrometric accuracy of IXPE does not allow for a clean spatial separation of these two components, but a combination of IXPE data with the high spatial resolution of Chandra and XMM-Newton and Chandra spectra can be used to constrain their contributions. This will be reported elsewhere.

We conclude by saying that IXPE observations show that X-ray emission from G0.13-0.11 is strongly polarized ($\sim 60\%$) in the direction perpendicular to the bright Wings-like X-ray structure and to the trailing radio-emitting filaments, which are part of the Galactic Center Radio Arc. While the IXPE angular resolution is not sufficient to spatially resolve polarized emission into individual sub-arcmin components, i.e. the "Wings" and the fainter diffuse emission to the east of the "Wings", the statement of the high degree of polarization is robust. These measurements demonstrate that X-ray threads in GC regions are produced by synchrotron emission of $\sim$ 10 TeV leptons gyrating in the ordered magnetic field perpendicular to the Galactic Plane.

ACKNOWLEDGEMENTS

The Imaging X-ray Polarimetry Explorer (IXPE) is a joint US and Italian mission. The US contribution is supported by the National Aeronautics and Space Administration (NASA) and led and managed by its Marshall Space Flight Center (MSFC), with industry partner Ball Aerospace (contract NNM15AA18C). The Italian contribution is supported by the Italian Space Agency (Agenzia Spaziale Italiana, ASI) through contract ASI-OHBI-2022-13-I.0, agreements ASI-INAF-2022-19-HH.0 and ASI-INFN-2017.13-H0, and its Space Science Data Center (SSDC) with agreements ASI-INAF-2022-14-HH.0 and ASI-INFN 2021-43-HH.0, and by the Istituto Nazionale di Astrofisica (INAF) and the Istituto Nazionale di Fisica Nucleare (INFN) in Italy. This research used data products provided by the IXPE Team (MSFC, SSDC, INAF, and INFN) and distributed with additional software tools by the High-Energy Astrophysics Science Archive Research Center (HEASARC), at NASA Goddard Space Flight Center (GSFC).

IK acknowledges support by the COMPLEX project from the European Research Council (ERC) under the European Union's Horizon 2020 research and innovation program grant agreement ERC-2019-AdG 882679. RK, AV, and WF acknowledge support from the Smithsonian Institution, the High Resolution Camera Project through NASA contract NAS8-03060, and Chandra grant GO1-22136X. NB is supported by the INAF MiniGrant "PWNnumpol - Numerical Studies of Pulsar Wind Nebulae in The Light of IXPE".

The MeerKAT telescope is operated by the South African Radio Astronomy Observatory, which is a facility of the National Research Foundation, an agency of the Department of Science and Innovation.

REFERENCES

Abdollahi S., et al., 2020, ApJS, 247, 33
Bandiera R., 2008, A&A, 490, L3
Bandiera R., Petruk O., 2016, MNRAS, 459, 178
Barkov M. V., Lyutikov M., Khangulyan D., 2019, MNRAS, 484, 4760
Beck R., Krause M., 2005, Astronomische Nachrichten, 326, 414
Brienza M., et al., 2021, Nature Astronomy, 5, 1261
Bykov A. M., Amato E., Petrov A. E., Krassilchtchikov A. M., Levenfish K. P., 2017, SSRv, 207, 235
Churazov E., Sunyaev R., Sazonov S., 2002, MNRAS, 330, 817
Churazov E., Khabibullin I., Bykov A. M., Lyskova N., Sunyaev R., 2023, A&A, 670, A156
Di Marco A., et al., 2023, AJ, 165, 143
Gaensler B. M., Slane P. O., 2006, ARA&A, 44, 17
H. E. S. S. Collaboration et al., 2018, A&A, 612, A9
Heywood I., et al., 2019, Nature, 573, 235
Heywood I., et al., 2022, ApJ, 925, 165
Kargaltsev O., Pavlov G. G., Klingler N., Rangelov B., 2017, Journal of Plasma Physics, 83, 635830501
Kislat F., Clark B., Beilicke M., Krawczynski H., 2015, Astroparticle Physics, 68, 45
Koyama K., Maeda Y., Sonobe T., Takeshima T., Tanaka Y., Yamauchi S., 1996, PASJ, 48, 249
LaRosa T. N., Nord M. E., Lazio T. J. W., Kassim N. E., 2004, ApJ, 607, 302
Lang C. C., Morris M., Echevarria L., 1999, ApJ, 526, 727
Longair M. S., 2011, High Energy Astrophysics
Marin F., et al., 2023, Nature, 619, 41
Markevitch M., Sunyaev R. A., Pavlinsky M., 1993, Nature, 364, 40
Matt G., 2004, A&A, 423, 495
Morris M., 2006, in Journal of Physics Conference Series. pp 1–9, doi:10.1088/1742-6596/54/1/001
Muno M. P., et al., 2009, ApJS, 181, 110
Niederwanger F., Reimer O., Kissmann R., Strong A. W., Popescu C. C., Tuffs R., 2019, Astroparticle Physics, 107, 1
Olmi B., Bucciantini N., 2019, MNRAS, 490, 3608
Olmi B., Bucciantini N., 2023, PASA, 40, e007
Paré D. M., Lang C. C., Morris M. R., Moore H., Mao S. A., 2019, ApJ, 884, 170
Paré D. M., Purcell C. R., Lang C. C., Morris M. R., Green J. A., 2021, ApJ, 923, 82
Pavan L., Bozzo E., Pühlhofer G., Ferrigno C., Balbo M., Walter R., 2011, A&A, 533, A74
Popescu C. C., Yang R., Tuffs R. J., Natale G., Rushton M., Aharonian F., 2017, MNRAS, 470, 2539
Rajpurohit K., et al., 2020, A&A, 636, A30
Revnivtsev M., Sazonov S., Churazov E., Forman W., Vikhlinin A., Sunyaev R., 2009, Nature, 458, 1142
Rudnick L., et al., 2022, ApJ, 935, 168
Sunyaev R. A., Markevitch M., Pavlinsky M., 1993, ApJ, 407, 606
Tsuboi M., Inoue M., Handa T., Tabara H., Kato T., Sofue Y., Kaifu N., 1986, AJ, 92, 818
Vainshtein L. A., Sunyaev R. A., 1980, Soviet Astronomy Letters, 6, 353
Vikhlinin A., et al., 2009, ApJ, 692, 1033
Wang Q. D., Lu F., Lang C. C., 2002, ApJ, 581, 1148
Weisskopf M. C., et al., 2022, Journal of Astronomical Telescopes, Instruments, and Systems, 8, 026002
Yusef-Zadeh F., Morris M., Chance D., 1984, Nature, 310, 557
Yusef-Zadeh F., Law C., Wardle M., 2002, ApJL, 568, L121
Yusef-Zadeh F., Hewitt J. W., Cotton W., 2004, ApJS, 155, 421
Zhang S., et al., 2020, ApJ, 893, 3
de Vries M., et al., 2022, ApJ, 939, 70